Schweizerischer Erdbebendienst
Service Sismologique Suisse
Servizio Sismico Svizzero
Servizi da Terratrembels Svizzer

ETH
Eidgenössische Technische Hochschule Zürich
Swiss Federal Institute of Technology Zurich

Reinach - Rainenweg (SRER)

SITE CHARACTERIZATION REPORT

Clotaire MICHEL, Valerio POGGI, Carlo CAUZZI,

Jan BURJANEK, Daniel ROTEN, Donat FÄH

Sonneggstrasse 5 CH-8092 Zürich Switzerland; E-mail: clotaire.michel@sed.ethz.ch

Last modified : November 5, 2013

Abstract

Ambient vibration array measurements were performed on the alluvial site of Reinach Rainenweg. The site, where the new station SRER of the Swiss Strong Motion Network was installed, is close to the fault of Reinach, most likely associated to the 1356 Mw=6.8 Basel earthquake. SRER replaces the dial-up station SRNR. In order to characterize the velocity profile under the station, array measurements with a $120\,\mathrm{m}$ aperture were performed. The measurements were successful and allowed deriving a velocity model for this site. Furthermore, a comparison with borehole data was possible at this site. The soil column underlying station SRER is made of a first layer of consolidated sediments of about $30\,\mathrm{m}$ with a shear wave velocity around $550\,\mathrm{m/s}$ that may correspond to quaternary alluvial terraces and the Tüllinger layer. Below, the Molasse alsacienne shows increasing velocities and a strong interface at $100\,\mathrm{m}$ where the velocity jumps to $1100\,\mathrm{m/s}$. The lower layers are not constrained by the data down to the bedrock at $570\,\mathrm{m}$ determined from borehole data. The fundamental frequency at this site is $0.45\,\mathrm{Hz}$. 2D phenomena are expected in the valley, though pure 2D resonance was excluded. $V_{s,30}$ is found to be $514\,\mathrm{m/s}$, corresponding to ground type B in Eurocode 8 ([CEN, 2004]). Both the theoretical SH transfer function and the quarter-wavelength proxy for amplification suggest amplification with respect to the local rock of about 3, especially at resonance frequencies. Recordings of the new station will allow to validate these simple models.

Contents

1 Introduction

The station SRER (Reinach Rainenweg) is part of the Swiss Strong Motion Network (SSMNet) in the Basel region. SRER has been installed in the framework of the SSMNet Renewal project in 2011, replacing the SRNR (Reinach Reinacherhof) dial-up station. This project includes also the site characterization. The passive array measurement has been selected as a standard tool to investigate these sites. Such a measurement campaign was carried out on 7th April 2011 in Reinach Rainenweg (Fig. 1), 50 m away from station SRER, in order to characterize the sediments under this station. The station is 100 m away from the basin edge bordered by the Reinach fault, where trenching was performed some years ago, since it is most likely associated to the 1356 Mw=6.8 Basel earthquake [Fäh et al., 2009a]. This report presents the measurement setup, the results of the H/V analysis and of the array processing of the surface waves aimed at estimating the dispersion curves. Comparison with other experiments close to SRNR station, including a borehole is also presented. Then, an inversion of these results for a velocity profile is performed. Standard parameters are derived to evaluate the amplification at this site.

Canton	City	Location	Station code	Site type	Slope
Basel Land	Reinach	Rainenweg	SRER	Plain	Flat

Table 1: Main characteristics of the study-site.

Figure 1: Picture of the site.

2 Experiment description

2.1 Ambient Vibrations

The ground surface is permanently subjected to ambient vibrations due to:

- natural sources (ocean and large-scale atmospheric phenomena) below $1\,\mathrm{Hz}$,
- local meteorological conditions (wind and rain) at frequencies around $1\,\mathrm{Hz}$,
- human activities (industrial machines, traffic…) at frequencies above $1\,\mathrm{Hz}$ [Bonnefoy-Claudet et al., 2006].

The objective of the measurements is to record these ambient vibrations and to use their propagation properties to infer the underground structure. First, the polarization of the recorded waves (H/V ratio) is used to derive the resonance frequencies of the soil column. Second, the arrival time delays at many different stations are used to derive the velocity of surface waves at different frequencies (dispersion). The information (H/V, dispersion curves) is then used to derive the properties of the soil column using an inversion process.

2.2 Equipment

For these measurements, 11 Quanterra Q330 dataloggers named NR02 to NR12 and 14 Lennartz 3C 5 s seismometers were available (see Tab. 2). Each datalogger can record on 2 ports A (channels EH1, EH2, EH3 for Z, N, E directions) and B (channels EH4, EH5, EH6 for Z, N, E directions). Time synchronization was ensured by GPS. The sensor were placed on a metal tripod in a $20\,\mathrm{cm}$ deep hole, when possible, for better coupling with the ground.

Digitizer	**Model**	**Number**	**Resolution**
	Quanterra Q330	11	$24\,\mathrm{bits}$
Sensor type	**Model**	**Number**	**Cut-off frequency**
Velocimeter	Lennartz 3C	14	$0.2\,\mathrm{Hz}$

Table 2: Equipment used.

2.3 Geometry of the arrays

Two array configurations were used, for a total of 4 rings of 10, 20, 40 and $60\,\mathrm{m}$ radius around a central station. The first configuration includes the 3 inner rings with 14 sensors; the second configuration includes the 2 outer rings with 11 sensors with two additional sensors of the first two rings that were not removed. The minimum inter-station distance and the aperture are therefore 10 and $80\,\mathrm{m}$ and 10 and $120\,\mathrm{m}$, respectively. The experimental setup is displayed in Fig. 2. The final usable datasets are detailed in section 3.2.

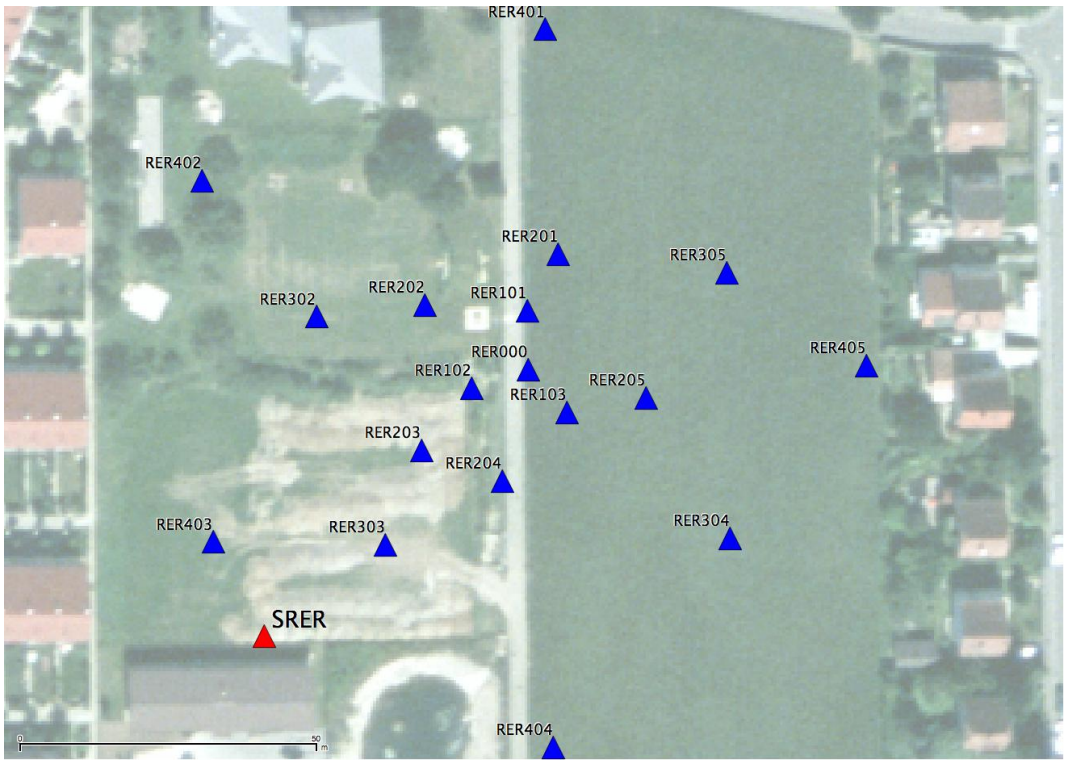

Figure 2: Geometry of the arrays.

2.4 Positioning of the stations

The sensor coordinates of the array were measured using a differential GPS device (Leica Viva), including only a rover station and using the Real Time Kinematic technique provided by Swisstopo. It allows an absolute positioning with an accuracy of about $3\,\mathrm{cm}$ on the Swissgrid.

3 Data quality

3.1 Usable data

The largest time windows were extracted, for which all the sensors of the array were in position and the GPS synchronization was ensured. Moreover, after 16:00 local time, kids started to play close to sensors RER403 (on the football field) and RER303 (on the bike lane) and a large truck carrying sand crossed the array so that the measurement was stopped and the last minutes were cut. The characteristics of the datasets are detailed in Tab. 3.
Station NR12 (point RER301) did not record because the Baler was set in "format" mode.

Moreover, it should be noticed that a M=6.3 earthquake in Mexico was recorded at 13:23:40 by the second configuration of the array. This dataset is not processed in this report.

3.2 Data processing

The data were first converted to SAC format, including in the header the sensor coordinates (CH1903 system), the recording component and a name related to the position of the station. The name is made of 3 letters characterizing the location (RER here), 1 digit for the ring and 2 more digits for the number in the ring. Recordings were not corrected from the instrumental response.

Dataset	**Starting Date**	**Time**	**Length**	F_s	**Min. inter-distance**	**Aperture**	**# of points**
1	2011/04/07	10:22	93 min	200 Hz	10 m	80 m	13
2	2011/04/07	12:39	96 min	200 Hz	10 m	120 m	12
EQ	2011/04/07	13:23	5 min	200 Hz	10 m	120 m	12

Table 3: Usable datasets.

4 H/V processing

4.1 Processing method and parameters

In order to process the H/V spectral ratios, several codes and methods were used. The classical H/V method was applied using the Geopsy `http://www.geopsy.org` software. In this method, the ratio of the smoothed Fourier Transform of selected time windows are averaged. Tukey windows (cosine taper of 5% width) of $50\,\mathrm{s}$ long overlapping by 50% were selected. Konno and Ohmachi [1998] smoothing procedure with b=80 was used. The classical H/V of Fäh et al. [2001] was also applied.

Moreover, the time-frequency analysis method [Fäh et al., 2009b] was used to estimate the ellipticity function more accurately using the Matlab code of V. Poggi, available in the software repository of the engineering seismology group of SED. In this method, the time-frequency analysis using the Wavelet transform is computed for each component. For each frequency, the maxima over time (10 per minute with at least $0.1\,\mathrm{s}$ between each) in the TFA are determined. The Horizontal to Vertical ratio of amplitudes for each maximum is then computed and statistical properties for each frequency are derived. A Cosine wavelet with parameter 9 was used. The mean of the distribution for each frequency is stored. For the sake of comparison, the time-frequency analysis of Fäh et al. [2001], based on the spectrogram, was also used, as well as the wavelet-based TFA coded in Geopsy.

The ellipticity was also extracted using the Capon analysis [Poggi and Fäh, 2010] (see section on 3C array analysis) and also plotted on Fig. 4. The results are coherent even if the low frequency part is missing due to the too low array aperture.

Method	Freq. band	Win. length	Anti-trig.	Overlap	Smoothing
Standard H/V Geopsy	$0.2 - 20\,\mathrm{Hz}$	$50\,\mathrm{s}$	No	50%	K&O 80
Standard H/V D. Fäh	$0.2 - 20\,\mathrm{Hz}$	$30\,\mathrm{s}$	No	75%	?
H/V TFA Geopsy	$0.2 - 20\,\mathrm{Hz}$	Morlet m=8 fi=1	No	-	?
H/V TFA D. Fäh	$0.2 - 20\,\mathrm{Hz}$	Specgram	No	-	?
H/V TFA V. Poggi	$0.2 - 20\,\mathrm{Hz}$	Cosine wpar=9	No	-	No

Table 4: Methods and parameters used for the H/V processing.

4.2 Results

H/V curves are consistent for all the recordings, except point RER204 that shows a slightly different behaviour probably due to bad ground coupling (Fig. 3). Moreover, all the methods to compute H/V ratios are compared on Fig. 4, in which the classical methods were arbitrarily divided by $\sqrt{2}$. The matching above the resonance frequency is good except smoothing issues. However, the peak is not easy to determine between 0.4 and $0.75\,\mathrm{Hz}$, on average $0.45\,\mathrm{Hz}$, with a peak amplitude around 3.

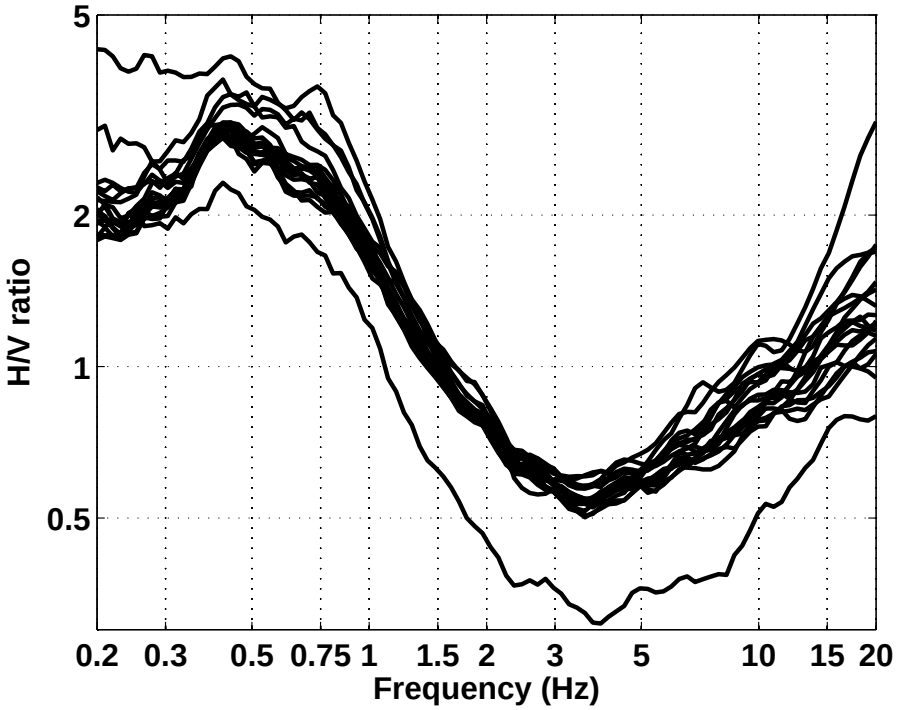

Figure 3: H/V spectral ratios (time-frequency analysis code V. Poggi).

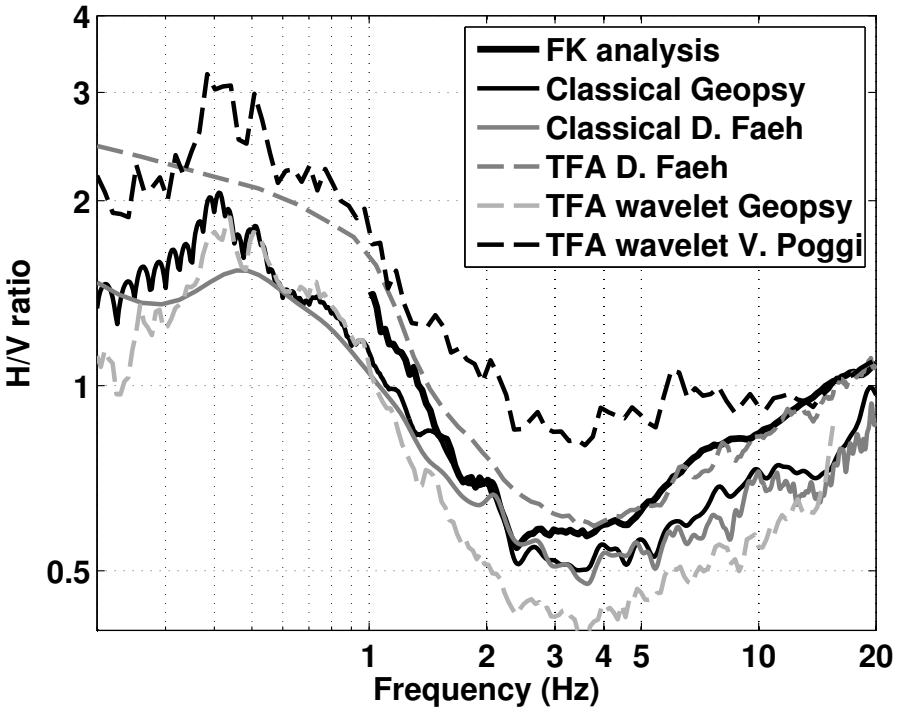

Figure 4: H/V spectral ratios for point RER000 using the different codes. Classical methods were divided by $\sqrt{2}$.

4.3 Polarization analysis

Since the frequency 0.45 Hz can be found on a large area, a polarization analysis using the code of Burjánek et al. [2010] was performed in order to determine if it is related to 2D resonance. The results shows no polarization of the ground motion at this frequency with a preferential direction (Fig. 5). This resonance does therefore not correspond to a pure 2D resonance but 2D effects are not excluded. Steimen et al. [2003] showed that 2D resonance could occur in this site using modeling but could not find 2D resonance peaks as well using data.

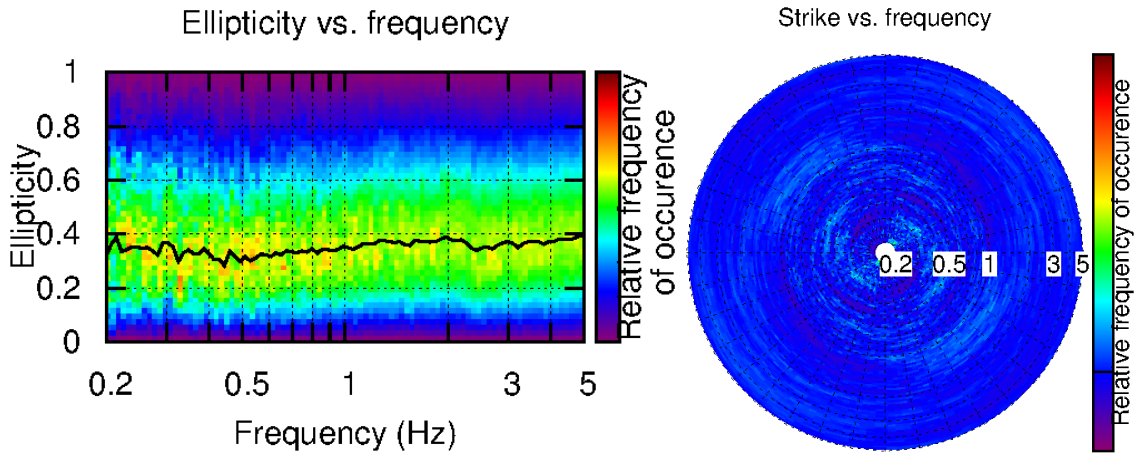

Figure 5: Polarization analysis at point RER000. Left: Ellipticity (A trough in the ellipticity corresponds to polarized motion). Right: Strike of the polarization.

5 Array processing

5.1 Processing methods and parameters

The vertical components of the arrays were processed using the High-resolution FK analysis [Capon, 1969] using the Geopsy `http://www.geopsy.org` software. Better results were obtained using large time windows (500T). The results in the FK plane were concatenated.

Moreover, a 3C array analysis [Fäh et al., 2008] was also performed using the Array Tool 3C software [Poggi and Fäh, 2010] using the Capon SVD method. It allows to derive Rayleigh and Love modes. The results of computations of both datasets were merged to estimate the dispersion curves.

Method	Set	Freq. band	Win. length	Anti-trig.	Overlap	Grid step	Grid size	# max.
HRFK 1C	1	$0.5 - 30\,\mathrm{Hz}$	$500T$	No	50%	0.001	0.5	5
HRFK 1C	2	$0.5 - 30\,\mathrm{Hz}$	$500T$	No	50%	0.001	0.5	5
HRFK 3C	1	$0.8 - 30\,\mathrm{Hz}$	$20T$ Tap. 0.1	No	5%	300 m/s	3000 m/s	5
HRFK 3C	2	$0.8 - 30\,\mathrm{Hz}$	$20T$ Tap. 0.1	No	5%	300 m/s	3000 m/s	5

Table 5: Methods and parameters used for the array processing.

5.2 Obtained dispersion curves

Both 1C (Fig. 6) and 3C (Fig. 7) analyses provided similar results. The Rayleigh fundamental mode could be picked between 2 and $25\,\mathrm{Hz}$ including its standard deviation. The dispersion curve can be followed below the lower array limit thanks to the Capon technique. Looking at the k-plane, the resolution is good enough down to $2\,\mathrm{Hz}$ (probably below but we decided to stop at this frequency). Velocities range from $950\,\mathrm{m/s}$ at $2\,\mathrm{Hz}$ down to $470\,\mathrm{m/s}$ at $25\,\mathrm{Hz}$. Directionality was investigated, separating the signals coming from the Reinach fault (90 to 210 °) and signal going to the fault (270 to 30°). However, no relevant difference could be observed.

Moreover, the SVD method allowed to derive the ellipticity of the Rayleigh mode [Poggi and Fäh, 2010], with resolution down to $1\,\mathrm{Hz}$ only. It compares well to the H/V ratios, with a lower standard deviation.

The radial component shows the Rayleigh mode as well, but with low accuracy close to the array limit. It was not used in the picking.

The transverse component allows to pick the fundamental Love mode between 2 and $29\,\mathrm{Hz}$ including its standard deviation (Fig. 7). The portion above $7\,\mathrm{Hz}$ is well defined, whereas at lower frequency, especially between 3 and $7\,\mathrm{Hz}$, the curve is not clear. Velocities range from $1300\,\mathrm{m/s}$ at $2\,\mathrm{Hz}$ down to $550\,\mathrm{m/s}$ at $29\,\mathrm{Hz}$.

The comparison (Fig. 9) with the array SRNR performed in 2000 [Kind, 2002] and located $500\,\mathrm{m}$ East shows a shift in the frequencies of the Rayleigh fundamental mode indicating probably a difference in the depth of the layers, the present study showing a deeper interface between the surface sediments and the layers below.

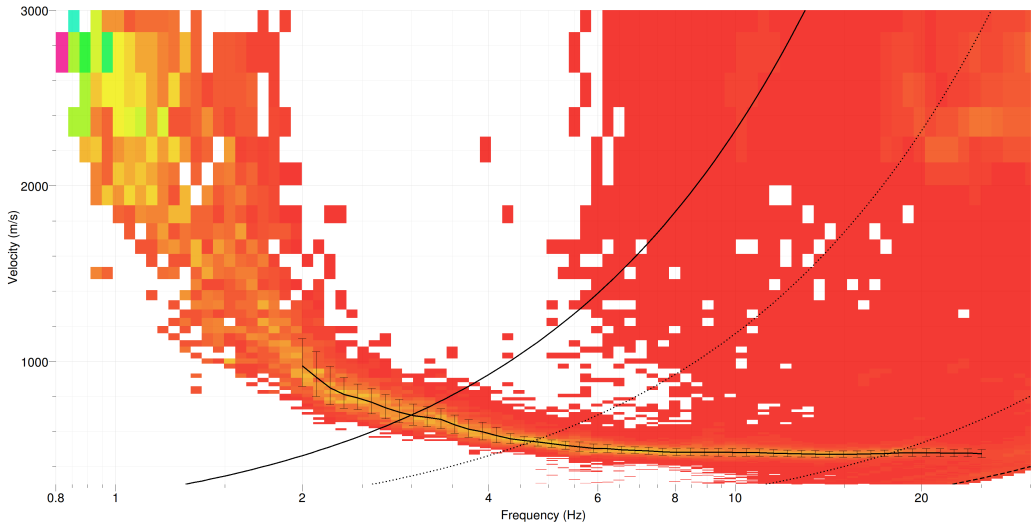

Figure 6: Dispersion curve obtained from the 1C array analysis.

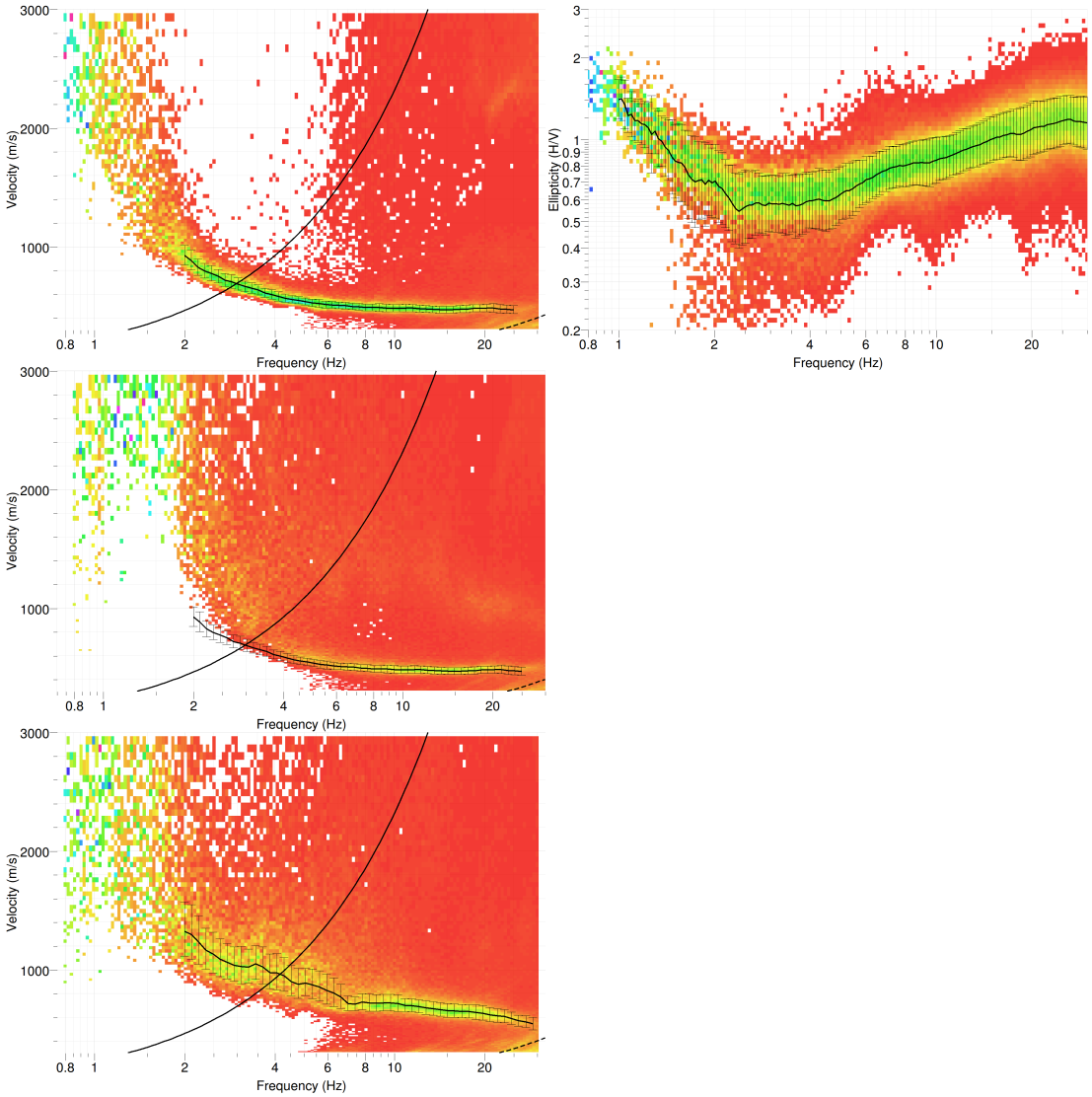

Figure 7: Dispersion curves (left) and ellipticity (right) obtained from the 3C array analysis. Top: Vertical - Centre: Radial - Bottom: Transverse component

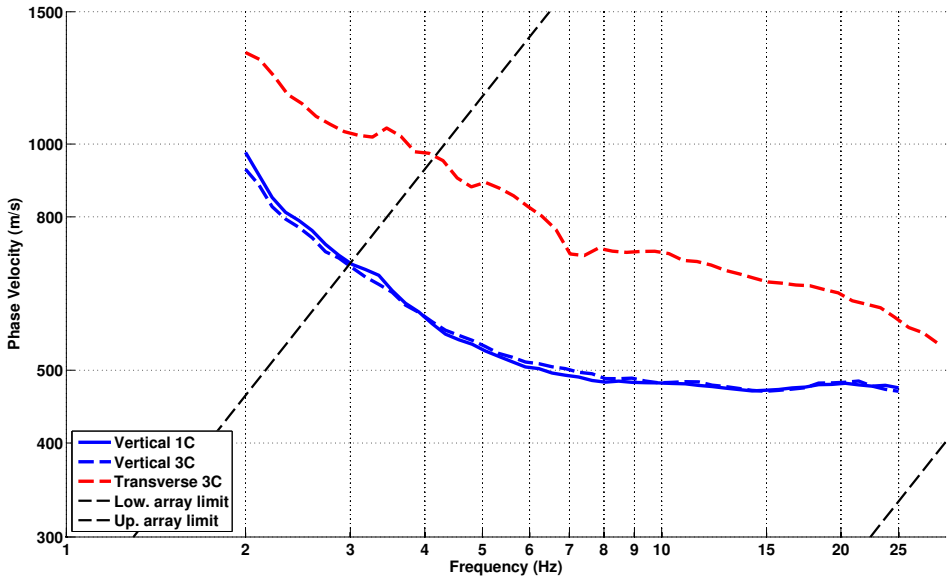

Figure 8: Picked dispersion curves from 1C and 3C analyses.

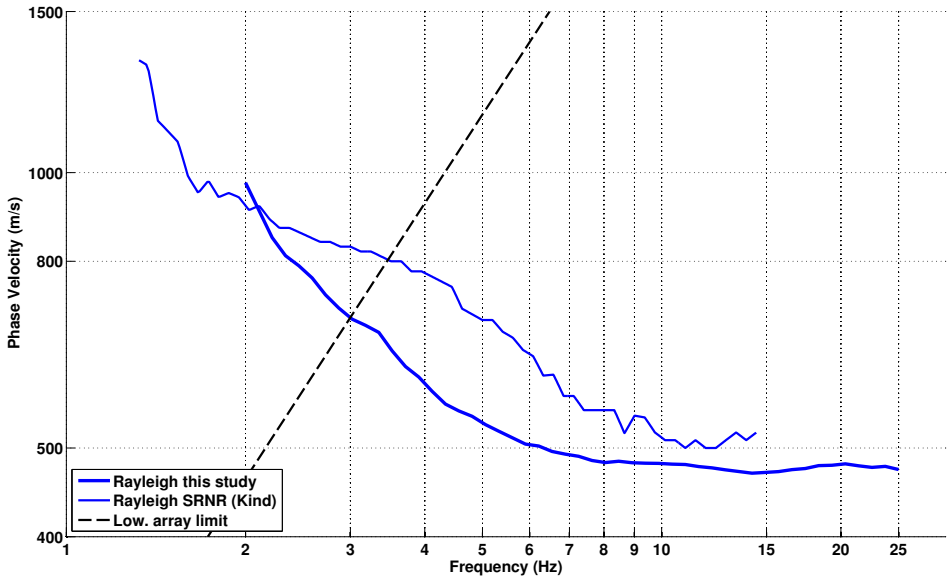

Figure 9: Comparison of the fundamental Rayleigh mode obtained by Kind [2002] at SRNR array and this study.

6 Borehole and existing model

Opršal et al. [2005] proposed a 3D model for the Basel region, largely based on the data of Kind [2002] (Fig. 9), located $500\,\mathrm{m}$ East (Fig. 10), and on the lithology at this site obtained from a borehole investigation [Hauber, 1991] (Fig. 11). A 1D profile was extracted from this model at the station SRER location and compared with the new data presented here. The dispersion and ellipticity of this model are computed and compared to the observations on Fig. 12 and Fig. 13.

The major result from this comparison is that the picked Love curve cannot correspond to the fundamental mode, but to a higher mode. Dispersion before and after $8\,\mathrm{Hz}$ is quite different and may be due to mixing the first and second higher Love modes. Therefore, only the part above $8\,\mathrm{Hz}$, most probably related to the first higher mode is kept.

Clear differences between the synthetic profile of Opršal et al. [2005] and the data presented here can be highlighted. The Rayleigh fundamental mode shows a slightly different behaviour indicating that the depths are not matching and the contrast around the array limit is also different from the one of the synthetic profile of Opršal et al. [2005].

Following the borehole [Hauber, 1991], Havenith and Fäh [2006] and Ripperger et al. [2009], we provide orders of magnitudes for the velocities of each layer on Tab. 6 for the Reinach site. The major velocity contrast (sediments/rock) occurs at $570\,\mathrm{m}$ depth, within the Rupelian age (Oligocene, Tertiary), between poorly consolidated marine sands and marls (named Sannoisian). From this table, it is clear that only small velocity contrasts occur within the sediments. The performed measurements are not able to validate or not the layering at greater depth provided by the different authors. It is moreover clear from Fig. 9 that the layering in SRNR (closer to the borehole) is different from the one in SRER.

Name	**Bottom depth [Opršal et al., 2005]**	**Bottom depth [Hauber, 1991]**	**Velocity range [Havenith and Fäh, 2006]**
Lower alluvial terrace	-	$13.4\,\mathrm{m}$	$400 - 700\,\mathrm{m/s}$
Tüllinger layer	$25\,\mathrm{m}$	$23\,\mathrm{m}$	$600 - 800\,\mathrm{m/s}$
Molasse alsacienne	$350\,\mathrm{m}$	$362\,\mathrm{m}$	$600 - 900\,\mathrm{m/s}$
Rupelian (Meletta layer etc.)	$600\,\mathrm{m}$	$570\,\mathrm{m}$	$600 - 1000\,\mathrm{m/s}$
Sannoisian marl	-	-	$1700 - 2500\,\mathrm{m/s}$

Table 6: Tuning parameters of Neighborhood Algorithm.

Figure 10: Map of previous array of Kind [2002] at SRNR site (light blue) and corresponding borehole Reinach 1 (light blue cross) [Hauber, 1991].

Tabelle 3: Die Bohrung Reinach 1. Schichteinfallen <10° aufgrund gezogener Kerne im Bereich 500—577 m, 642,6—650,0 m, 680,2—688,8 m, 740,0—749,0 m, 1059—1068,0 m, 1714,0—1723,0 m und 1740,0—1749,0 m.

Lokalität:	Sundgaustrasse, Reinach, Kt. Basel-Landschaft
Schweiz. Landeskoordination:	R = 612 524,55 H = 262 125,90
Greenwich Koordination:	λ = 7° 36′ 20″ E, φ = 47° 30′ 20″ N
Höhe:	292,13 m ü. NN
Bohrzeit:	03. 04. 1989 — 30. 06. 1989

Bohrprofil:

0	— 13,4	m	Niederterrassenschotter	Quartär
13,4	— 23	m	Tüllinger Schichten	Chattien
23	— 362	m	Molasse alsacienne	Chattien
362	— 515,6	m	Meletta-Schichten	Rupélien
515,6	— 535,8	m	Fischschiefer	Rupélien
535,8	— 563,8	m	Foraminiferenmegel	Rupélien
563,8	— 570,5	m	„Meeressand"	Rupélien
570,5	— 640	m	Obere Streifige Mergel	Sannoisien
640	— 727	m	Untere Streifige Mergel	Sannoisien
727	— 805	m	Rauracien-Korallenkalk	Oxfordien
805	— 829,5	m	Liesberg-Schichten	Oxfordien
829,5	— 889	m	Terrain à Chailles	Oxfordien
889	— 972	m	Renggeri-Tone	Oxfordien
972	—1029	m	Callovien und Varians-Schichten	Bathonien-Callovien
1029	—1157	m	Hauptrogenstein	Bajocien-Bathonien
1157	—1246	m	„Unterer Dogger"	Bajocien
1246	—1408	m	Opalinuston	Aalénien
1408	—1465	m	Lias	
1465	—1682	m	Rhät — Gipskeuper	Keuper
1682	—1697	m	Lettenkohle	Keuper
1697	—1714	m	Trigonodusdolomit	Ob. Muschelkalk
1714	—1770	m	Hauptmuschelkalk	Ob. Muschelkalk
1770	—1778	m	Dolomitzone	Mittl. Muschelkalk
1778	—1793,0	m	Sulfatzone	Mittl. Muschelkalk

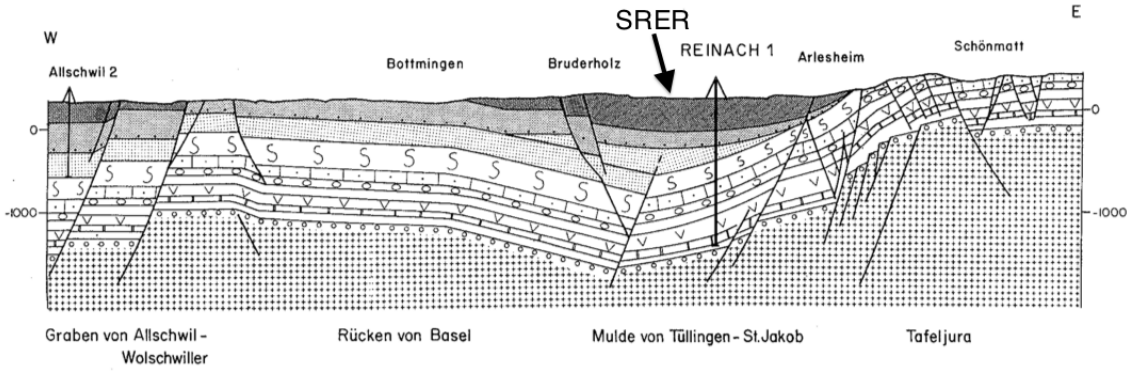

Figure 11: Borehole of Hauber [1991] and geological cross-section of the valley in Reinach.

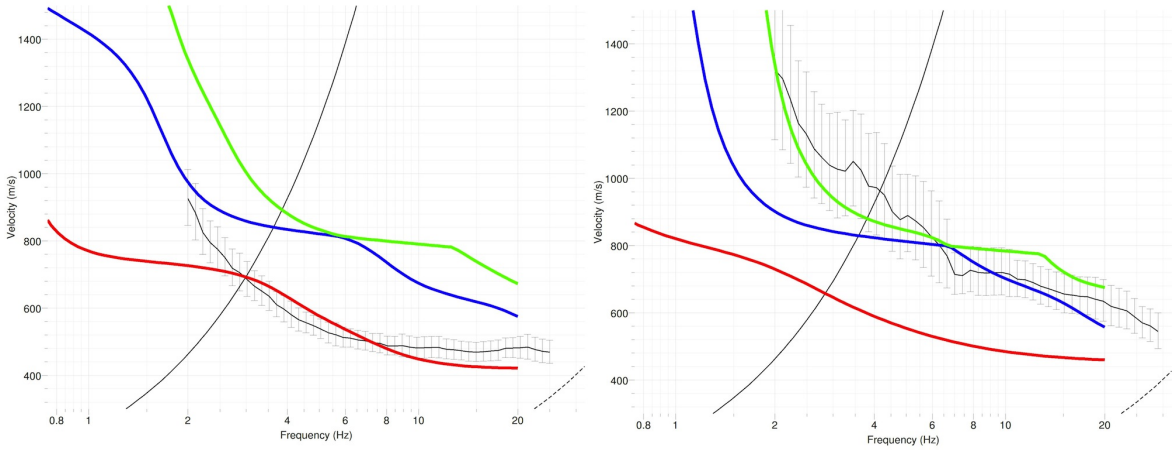

Figure 12: Comparison of the 3 first Rayleigh (left) and Love (right) modes (colored curves) extracted from Opršal et al. [2005] with the observed data (black curves with error bars).

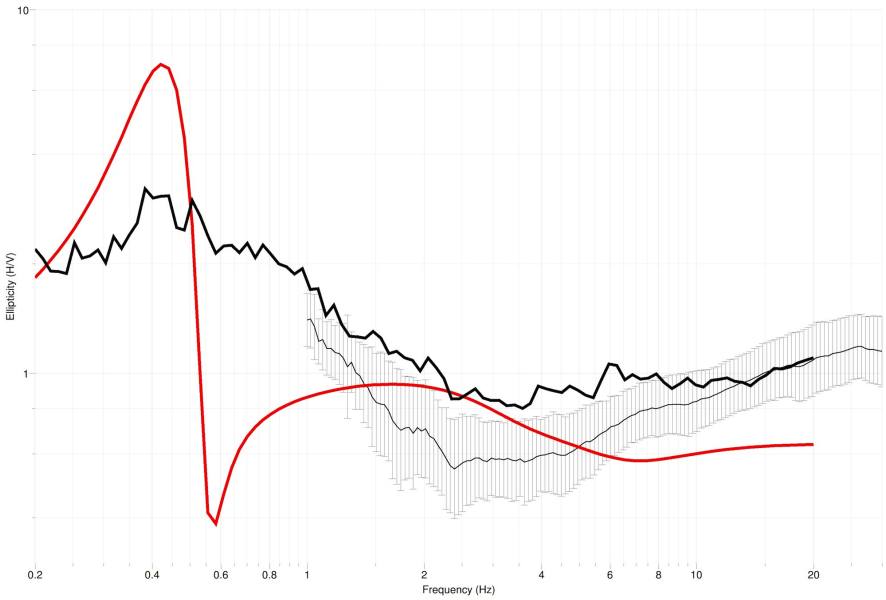

Figure 13: Comparison of the ellipticity of the Rayleigh waves extracted from Opršal et al. [2005] (red) and that derived from the observed data (black with error bounds: from the Capon technique; thick black line: H/V curve at RER000 - code V. Poggi)).

7 Inversion and interpretation

7.1 Inversion

For the inversion, the Rayleigh fundamental mode ($2 - 24\,\mathrm{Hz}$), the Love first higher mode ($8-27\,\mathrm{Hz}$), the ellipticity at high frequency ($6-30\,\mathrm{Hz}$) (3C FK analysis) and the ellipticity peak at $0.45\,\mathrm{Hz}$ were used as simultaneous targets. A weight of 0.2 was assigned to the ellipticity information. All curves were resampled using 80 points between 0.3 and $30\,\mathrm{Hz}$ in log scale. As shown in the previous section (Fig. 12) and after testing, the observed Love mode was considered as the first higher mode, which turned out to be a reasonable assumption. After extensive testing and comparison with recorded earthquakes, the right flank of the ellipticity was discarded. First of all, it could be related to 2D phenomena and moreover, not modeled rock layers may have a significant influence on it. The ellipticity peak is debatable as well, but no other constraint on the lower layers exist and it is absolutely needed to retrieve realistic profiles. Conversely, the high frequencies of the ellipticity were used to constrain better the upper layers.

The inversion was performed using the Improved Neighborhood Algorithm (NA) Wathelet [2008] implemented in the Dinver software. In this algorithm, the tuning parameters are the following: Ns_0 is the number of starting models, randomly distributed in the parameter space, Nr is the the number of best cells considered around these Ns_0 models, Ns is the number of new cells generated in the neighborhood of the Nr cells (Ns/Nr per cell) and It_{max} is the number of iteration of this process. The process ends with $Ns_0 + Nr * \frac{Ns}{Nr} * It_{max}$ models. The used parameters are detailed in Tab. 7.

It_{max}	Ns_0	Ns	Nr
500	10000	100	100

Table 7: Tuning parameters of Neighborhood Algorithm.

During the inversion process, low velocity zones were generally not allowed. Extensive testing showed that velocity inversions in the upper $35\,\mathrm{m}$ allowed to significantly better fit the dispersion curves, but since it did not allow to better fit the observed amplification function based on earthquake recordings, they are believed to correspond to over-fitting. As a result, velocity inversions probably occur in this zone, but our data is too sparse to constrain them. In order to explore the parameter space, one parametrization allowed for a velocity inversion. The Poisson ratio was inverted in the range 0.2-0.4 in each layer and the density was supposed equal to $2000\,\mathrm{kg/m^3}$ except for the deepest layer ($2500\,\mathrm{kg/m^3}$). Following a 1D profile extracted from the 3D model of Basel Opršal et al. [2005], the velocity of the deepest layer was set to $2000\,\mathrm{m/s}$ at $570\,\mathrm{m}$ depth [Hauber, 1991]. No constrain from the data is anyway available for the bedrock. Only few parameters were left free below $100\,\mathrm{m}$ since no data are constraining them. However, stopping the inversion at this depth would lead to large differences in the amplification function. Inversions with free layer depths as well as fixed layer depths were performed. 4 layers plus the bedrock are enough to explain all the targets (dispersion and ellipticity), but more layers are used to smooth the obtained results and better explore the parameter space. 5 independent runs of 5 different parametrization schemes (4, 5 and 6 layers over a half space and 12 and 14 layers

with fixed depth) were performed. For further elaborations, the best models of these 25 runs were selected (Fig. 17).

As explained above, the bedrock was set at $570\,\mathrm{m}$ depth with a velocity of $2000\,\mathrm{m/s}$. Above, a layer of velocities around $1100\,\mathrm{m/s}$ is found. No variations among this layer can be found with the data, but it is for sure at higher velocities than the Opršal et al. [2005] model (around $800\,\mathrm{m/s}$, Fig. 18). This is difficult to understand since the results of the array at SRNR [Kind, 2002] are not showing so low velocities at this depth and are closer to our results. The bottom part of the Kind [2002] profiles are more complex than those found here, it is difficult to say if they are realistic. In our inversion, a major interface occurs at $100\,\mathrm{m}$ depth, slightly deeper than the corresponding one at SRNR ($80\,\mathrm{m}$). Kind [2002] interprets it as the interface between the Molasse Alsacienne (below) and the Tüllinger layers (above), which is difficult to believe since Hauber [1991] found this interface at $23\,\mathrm{m}$ depth in the borehole. This is most likely an interface within the Molasse Alsacienne (weathering?). Above, the velocity is about $650\,\mathrm{m/s}$ up to $35\,\mathrm{m}$ depth. In this depth range, the velocity at SRNR is higher. Between 20 and $35\,\mathrm{m}$ depth, the situation is more chaotic due to the allowed velocity inversion. An interface around these depths (at $33\,\mathrm{m}$ depth according to the inversions without low-velocity zone) would match with the interface between the Molasse Alsacienne (below) and the Tüllinger layers (above). Above, the velocity stays relatively large up to the surface at about $540\,\mathrm{m/s}$. A $1\,\mathrm{m}$ layer at the surface with low velocity (V_s around $200 - 250\,\mathrm{m/s}$) helps the inversion.

The Love and Rayleigh dispersion curves show a good agreement with the target curves (Fig. 15, Fig. 16), but provide information only down to $75\,\mathrm{m}$. The $100\,\mathrm{m}$ interface, corresponding to about $1.5\,\mathrm{Hz}$, is not well constrained and may not be as sharp as found here. The reader is advised to use this information carefully. The bending of the dispersion curves can be better fitted with velocity inversions in the first $35\,\mathrm{m}$, but it seems it would be over-fitting the data.

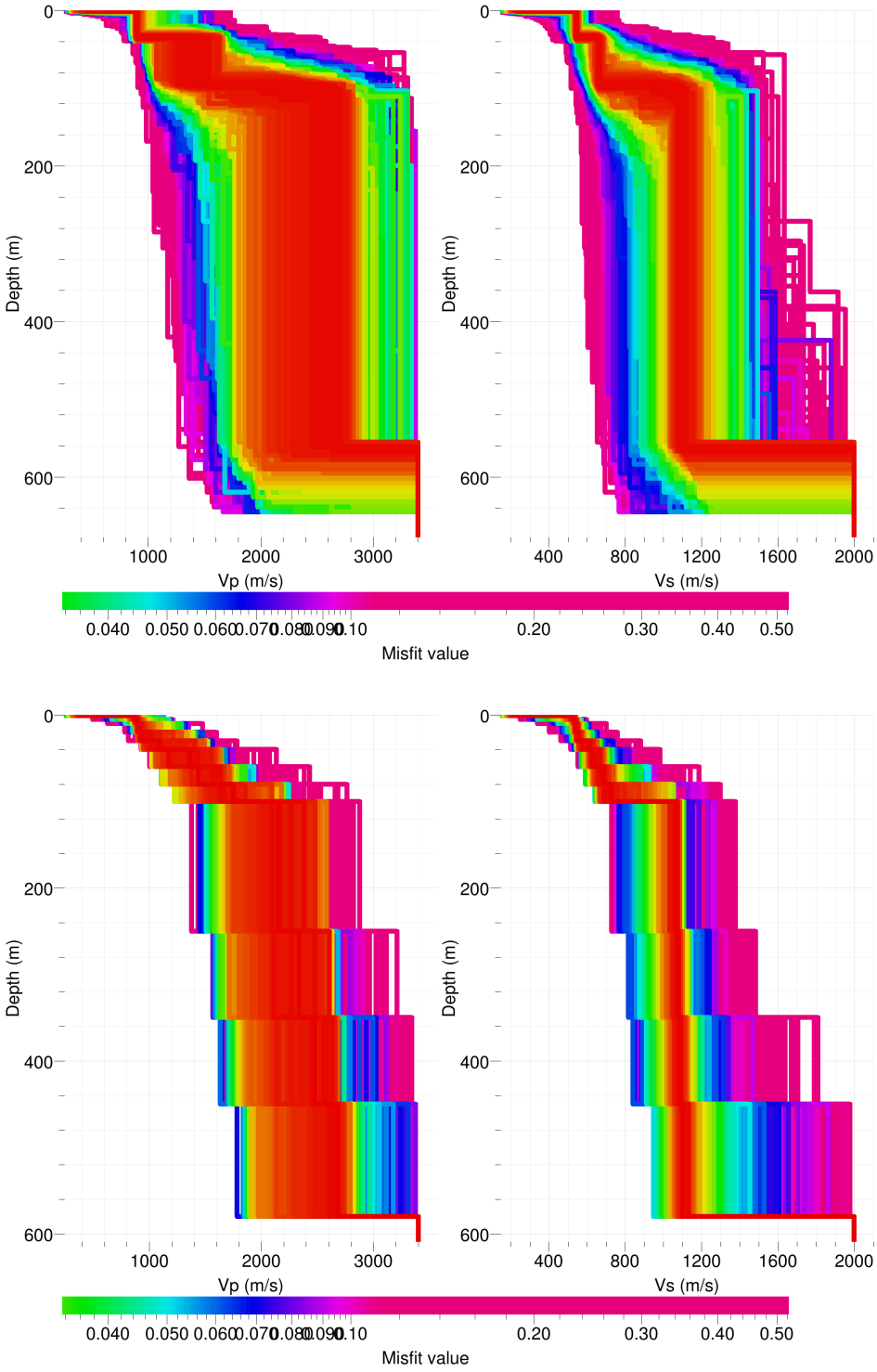

Figure 14: Inverted ground profiles in terms of V_p and V_s; top: free layer depth strategy; bottom: fixed layer depth strategy.

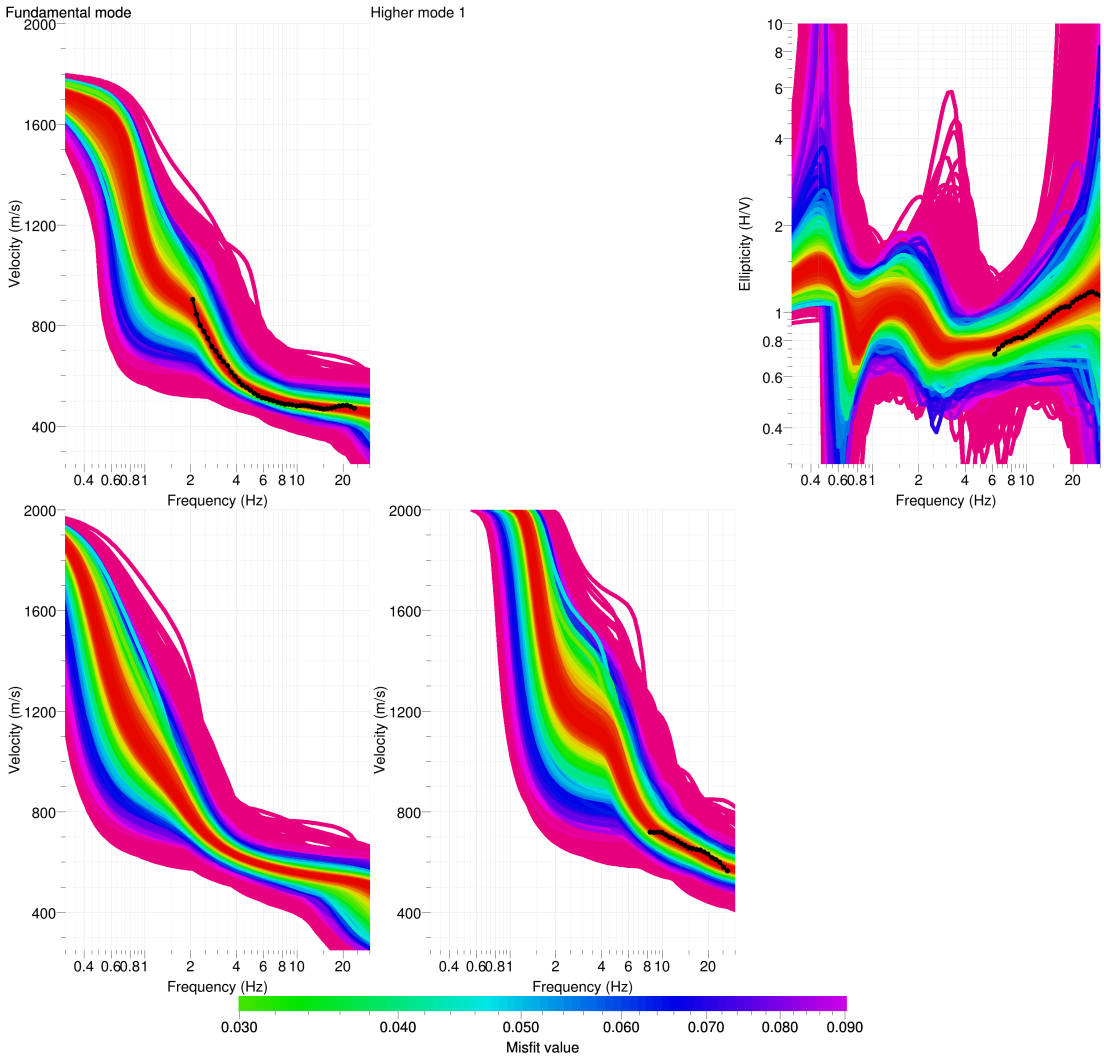

Figure 15: Comparison between inverted models and measured Rayleigh and Love modes and corresponding ellipticity, free layer depth strategy.

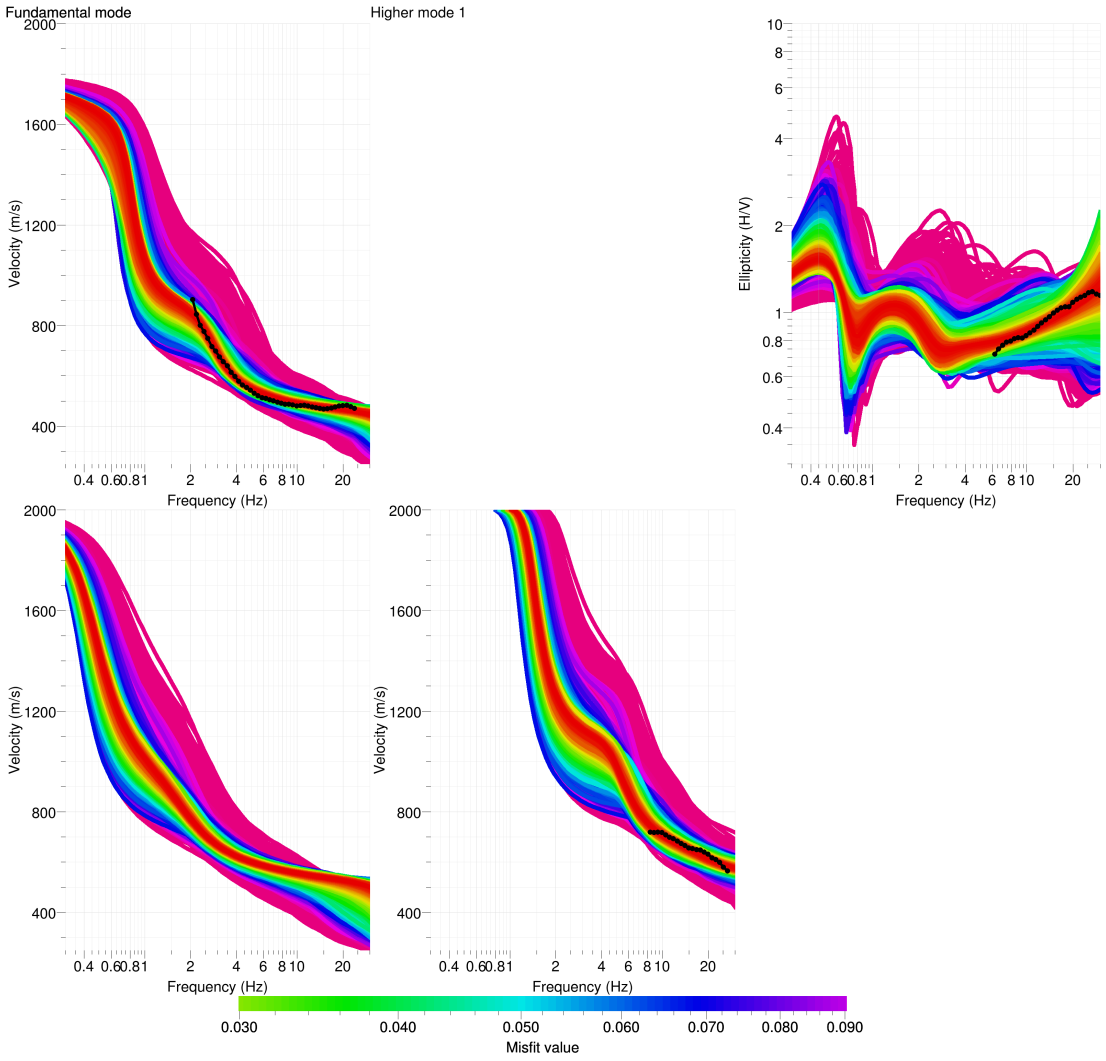

Figure 16: Comparison between inverted models and measured Rayleigh and Love modes and corresponding ellipticity, fixed layer depth strategy.

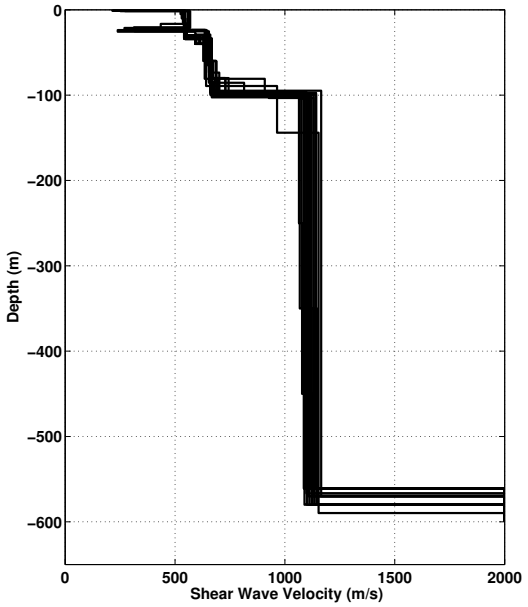

Figure 17: V_s ground profiles for the selected 25 best models.

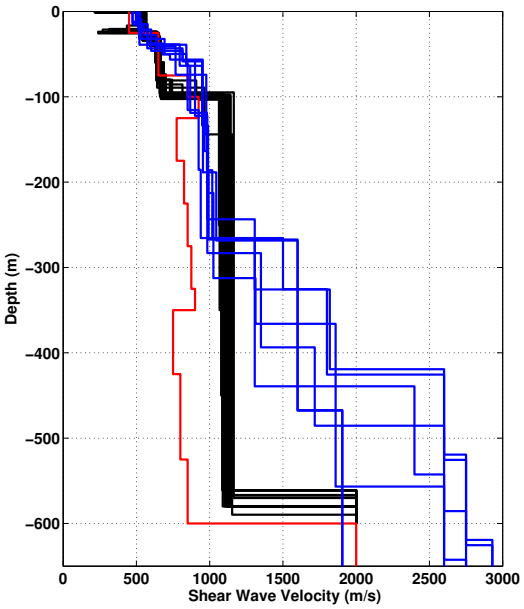

Figure 18: Comparison of the models retrieved here (black) with the profile extracted from Opršal et al. [2005] model (red) and the Kind [2002] results for SRNR array (blue).

7.2 Travel time average velocities and ground type

The distribution of the travel time average velocities at different depths was computed from the selected models. The uncertainty, computed as the standard deviation of the distribution of travel time average velocities for the considered models, is also provided, but its meaning is doubtful. $V_{s,30}$ is found to be $514\,\mathrm{m/s}$, meaning the site can be classified as class B in the Eurocode 8 [CEN, 2004] and SIA261 [SIA, 2003]. In the Swiss Code SIA261, this zone is part of the microzonation of Basel Zone Rheingraben Ost [Fäh and Huggenberger, 2006]. Amplifications around 2-3 in response spectra are proposed for this zone.

	Mean (m/s)	**Uncertainty (m/s)**
$V_{s,5}$	419	6
$V_{s,10}$	474	7
$V_{s,20}$	507	7
$V_{s,30}$	514	8
$V_{s,40}$	537	4
$V_{s,50}$	557	4
$V_{s,100}$	613	5
$V_{s,150}$	719	8
$V_{s,200}$	788	9

Table 8: Travel time averages at different depths from the inverted models. Uncertainty is given as one standard deviation from the selected profiles.

7.3 SH transfer function and quarter-wavelength velocity

The quarter-wavelength velocity approach [Joyner et al., 1981] provides, for a given frequency, the average velocity at a depth corresponding to 1/4 of the wavelength of interest. It is useful to identify the frequency limits of the experimental data (ellipticity peak $0.45\,\mathrm{Hz}$ and minimum frequency in the dispersion curves $2\,\mathrm{Hz}$). The results using this proxy show that the dispersion curves constrain the profiles down to $73\,\mathrm{m}$ and the ellipticity down to $560\,\mathrm{m}$ (Fig. 19). Moreover, the quarter wavelength impedance-contrast introduced by Poggi et al. [2012] is also displayed in the figure. It corresponds to the ratio between two quarter-wavelength average velocities, respectively from the top and the bottom part of the velocity profile, at a given frequency [Poggi et al., 2012]. It shows a trough (inverse shows a peak) at the resonance frequency.
Moreover, the theoretical SH-wave transfer function for vertical propagation [Roesset, 1970] is computed from the inverted profiles. It is compared to the quarter-wavelength amplification [Joyner et al., 1981] that however cannot take resonances into account (Fig. 20). In this case, the models are predicting an amplification up to a factor of 3 at several resonance peaks.

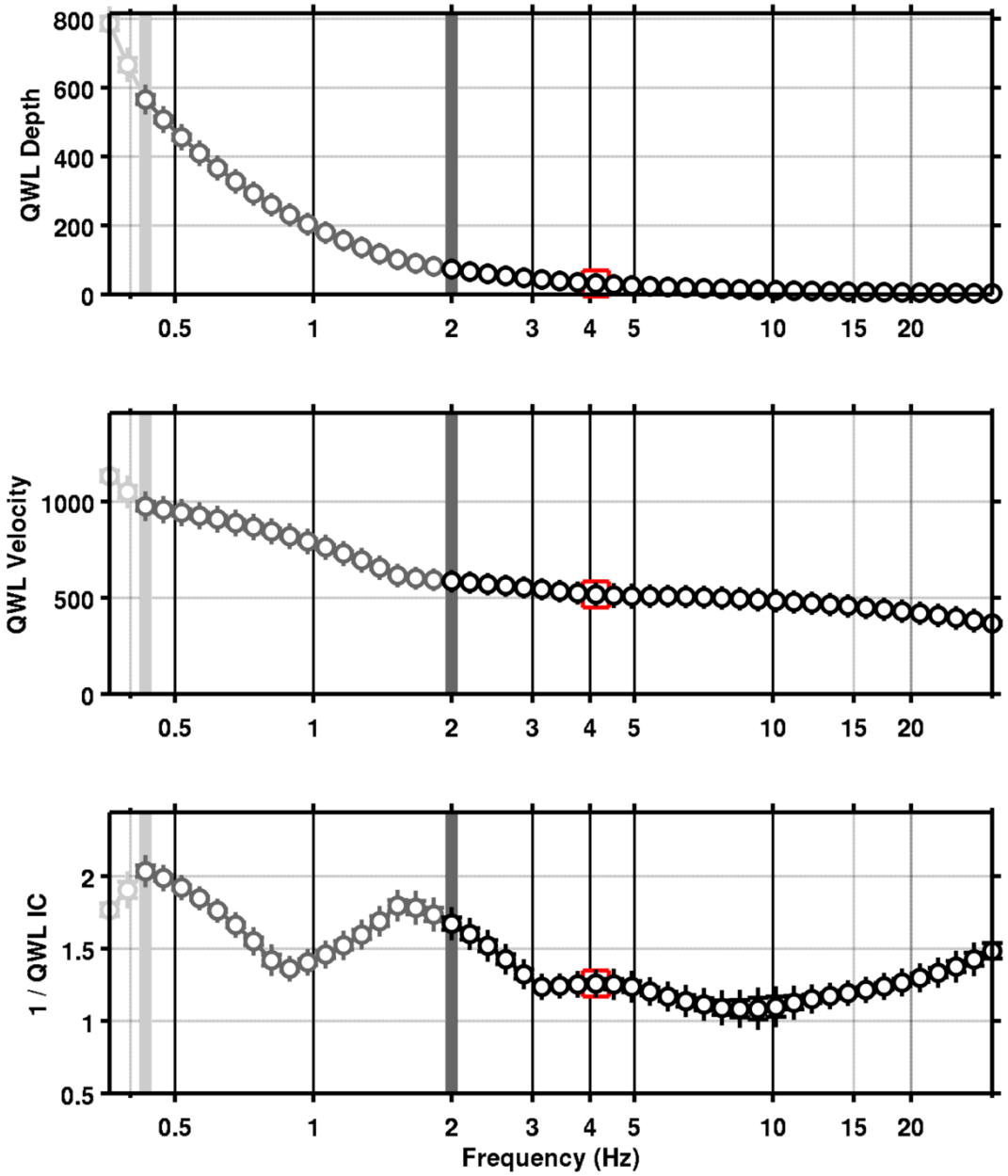

Figure 19: Quarter wavelength velocity representation of the velocity profile (top: depth, centre: velocity, bottom: inverse of the impedance contrast). Black curve is constrained by the dispersion curves, light grey is not constrained by the data. Red square is corresponding to $V_{s,30}$.

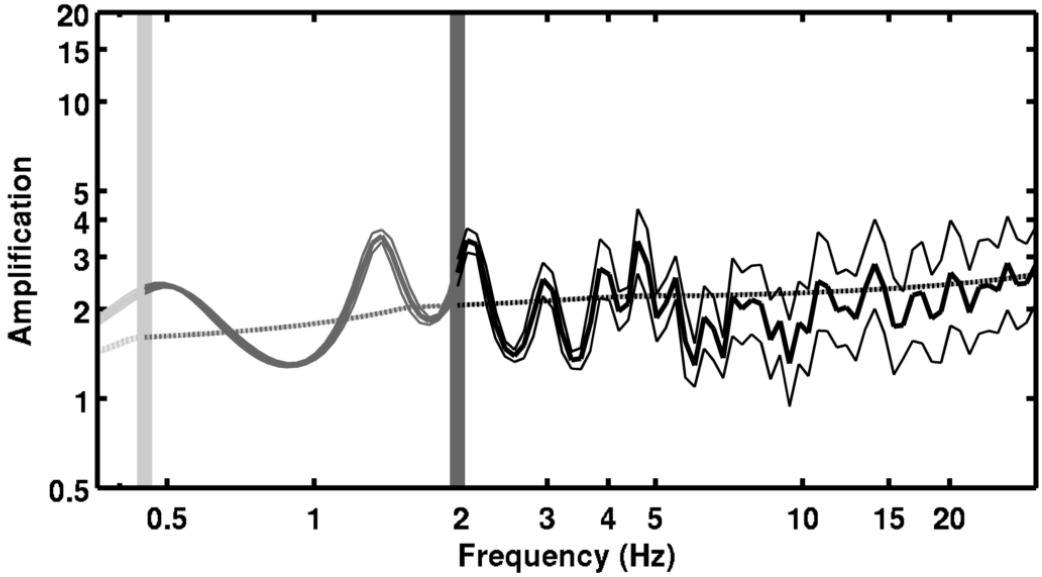

Figure 20: Theoretical SH transfer function (solid line) and quarter wavelength impedance contrast (dashed line) with their standard deviation. Significance of the greyshades is detailed in Fig. 19.

8 Conclusions

The array measurements presented in this study were successful in deriving a velocity model for the Birs valley in Reinach, below the SRER station. We found a first layer of consolidated sediments of about $30\,\mathrm{m}$ with a shear wave velocity around $550\,\mathrm{m/s}$ that may correspond to quaternary alluvial terraces and the Tüllinger layer. Below, the Molasse alsacienne shows increasing velocities and a strong interface at $100\,\mathrm{m}$ where the velocity jumps to $1100\,\mathrm{m/s}$. The lower layers are not constrain by the data down to the bedrock at $570\,\mathrm{m}$ determined from borehole data. The fundamental frequency at this site is $0.45\,\mathrm{Hz}$. 2D phenomena are expected in the valley, though pure 2D resonance was excluded. $V_{s,30}$ is found to be $514\,\mathrm{m/s}$. The theoretical SH transfer function and impedance contrast of the quarter-wavelength velocity computed from the inverted profiles agree on an amplification of 2 to 3 over a broad frequency range, particularly at resonance peaks. Recordings on the new station will allow to validate these simple models.

The recordings at station SRER will be very interesting to compare to the ones at station SRNR, in order to see if the proximity of the Reinach fault can be seen. It could then be possible, with station deployments, to determine if this fault is going on below the Basel city or not.

Acknowledgements

The authors thank Andreas Stutz for the help during these measurements.

References

Sylvette Bonnefoy-Claudet, Fabrice Cotton, and Pierre-Yves Bard. The nature of noise wavefield and its applications for site effects studies. *Earth-Science Reviews*, 79(3-4): 205–227, December 2006. ISSN 00128252. doi: 10.1016/j.earscirev.2006.07.004. URL http://linkinghub.elsevier.com/retrieve/pii/S0012825206001012.

Jan Burjánek, Gabriela Gassner-Stamm, Valerio Poggi, Jeffrey R. Moore, and Donat Fäh. Ambient vibration analysis of an unstable mountain slope. *Geophysical Journal International*, 180(2):820–828, February 2010. ISSN 0956540X. doi: 10.1111/j.1365-246X.2009.04451.x. URL http://doi.wiley.com/10.1111/j.1365-246X.2009.04451.x.

J. Capon. High-Resolution Frequency-Wavenumber Spectrum Analysis. *Proceedings of the IEEE*, 57(8):1408–1418, 1969.

CEN. *Eurocode 8: Design of structures for earthquake resistance - Part 1: General rules, seismic actions and rules for buildings*. European Committee for Standardization, en 1998-1: edition, 2004.

Donat Fäh and Peter Huggenberger. INTERREG III Projekt: Erdbebenmikrozonierung am südlichen Oberrhein. Zusammenfassung. Technical report, Eidgenössische Technische Hochschule Zürich (ETHZ), 2006.

Donat Fäh, Fortunat Kind, and Domenico Giardini. A theoretical investigation of average H / V ratios. *Geophysical Journal International*, 145:535–549, 2001.

Donat Fäh, Gabriela Stamm, and Hans-Balder Havenith. Analysis of three-component ambient vibration array measurements. *Geophysical Journal International*, 172(1):199–213, January 2008. ISSN 0956540X. doi: 10.1111/j.1365-246X.2007.03625.x. URL http://doi.wiley.com/10.1111/j.1365-246X.2007.03625.x.

Donat Fäh, Monika Gisler, Bernard Jaggi, Philipp Kästli, Thomas Lutz, Virgilio Masciadri, Christoph Matt, Dieter Mayer-Rosa, Dorothee Rippmann, Gabriela Schwarz-Zanetti, Jürg Tauber, and Thomas Wenk. The 1356 Basel earthquake: an interdisciplinary revision. *Geophysical Journal International*, 178(1):351–374, July 2009a. ISSN 0956540X. doi: 10.1111/j.1365-246X.2009.04130.x. URL http://gji.oxfordjournals.org/cgi/doi/10.1111/j.1365-246X.2009.04130.x.

Donat Fäh, Marc Wathelet, Miriam Kristekova, Hans-Balder Havenith, Brigitte Endrun, Gabriela Stamm, Valerio Poggi, Jan Burjanek, and Cécile Cornou. Using Ellipticity Information for Site Characterisation Using Ellipticity Information for Site Characterisation. Technical report, NERIES JRA4 Task B2, 2009b.

Lukas Hauber. Ergebnisse der Geothermiebohrungen Riehen 1 und 2 sowie Reinach 1 im Südosten des Rheingrabens. *Geologisches Jahrbuch*, E 48:167–184, 1991.

Hans-Balder Havenith and Donat Fäh. INTERREG III Projekt: Erdbebenmikrozonierung am südlichen Oberrhein. Teilbericht 2: Bestimmung der Scherwellengeschwindigkeiten. Technical report, Eidgenössische Technische Hochschule Zürich (ETHZ), 2006.

William B. Joyner, Richard E. Warrick, and Thomas E. Fumal. The effect of Quaternary alluvium on strong ground motion in the Coyote Lake, California, earthquake of 1979. *Bulletin of the Seismological Society of America*, 71(4):1333–1349, 1981.

Fortunat Kind. *Development of Microzonation Methods: Application to Basle, Switzerland*. PhD thesis, Swiss Federal Institute of Technology Zürich, 2002.

Katsuaki Konno and Tatsuo Ohmachi. Ground-Motion Characteristics Estimated from Spectral Ratio between Horizontal and Vertical Components of Microtremor. *Bulletin of the Seismological Society of America*, 88(1):228–241, 1998.

Ivo Opršal, Donat Fäh, P. Martin Mai, and Domenico Giardini. Deterministic earthquake scenario for the Basel area: Simulating strong motions and site effects for Basel, Switzerland. *Journal of Geophysical Research*, 110(B4):1–19, 2005. ISSN 0148-0227. doi: 10.1029/2004JB003188. URL http://www.agu.org/pubs/crossref/2005/2004JB003188.shtml.

Valerio Poggi and Donat Fäh. Estimating Rayleigh wave particle motion from three-component array analysis of ambient vibrations. *Geophysical Journal International*, 180(1):251–267, January 2010. ISSN 0956540X. doi: 10.1111/j.1365-246X.2009.04402.x. URL http://doi.wiley.com/10.1111/j.1365-246X.2009.04402.x.

Valerio Poggi, Benjamin Edwards, and D. Fah. Characterizing the Vertical-to-Horizontal Ratio of Ground Motion at Soft-Sediment Sites. *Bulletin of the Seismological Society of America*, 102(6):2741–2756, December 2012. ISSN 0037-1106. doi: 10.1785/0120120039. URL http://www.bssaonline.org/cgi/doi/10.1785/0120120039.

Johannes Ripperger, Philipp Kästli, Donat Fäh, and Domenico Giardini. Ground motion and macroseismic intensities of a seismic event related to geothermal reservoir stimulation below the city of Basel - observations and modelling. *Geophysical Journal International*, 179(3):1757–1771, December 2009. ISSN 0956540X. doi: 10.1111/j.1365-246X.2009.04374.x. URL http://gji.oxfordjournals.org/cgi/doi/10.1111/j.1365-246X.2009.04374.x.

J.M. Roesset. Fundamentals of soil amplification. In R. J. Hansen, editor, *Seismic Design for Nuclear Power Plants*, pages 183–244. M.I.T. Press, Cambridge, Mass., 1970. ISBN 978-0-262-08041-5. URL http://mitpress.mit.edu/catalog/item/default.asp?ttype=2\&tid=5998.

SIA. *SIA 261 Actions sur les structures porteuses*. Société suisse des ingénieurs et des architectes, Zürich, sia 261:20 edition, 2003.

Sibylle Steimen, Donat Fäh, Fortunat Kind, Christian Schmid, and Domenico Giardini. Identifying 2D Resonance in Microtremor Wave Fields. *Bulletin of the Seismological Society of America*, 93(2):583–599, 2003.

Marc Wathelet. An improved neighborhood algorithm: Parameter conditions and dynamic scaling. *Geophysical Research Letters*, 35(9):1–5, May 2008. ISSN 0094-8276. doi: 10.1029/2008GL033256. URL http://www.agu.org/pubs/crossref/2008/2008GL033256.shtml.